

Nanoscale

Accepted Manuscript



This is an *Accepted Manuscript*, which has been through the Royal Society of Chemistry peer review process and has been accepted for publication.

Accepted Manuscripts are published online shortly after acceptance, before technical editing, formatting and proof reading. Using this free service, authors can make their results available to the community, in citable form, before we publish the edited article. We will replace this *Accepted Manuscript* with the edited and formatted *Advance Article* as soon as it is available.

You can find more information about *Accepted Manuscripts* in the [Information for Authors](#).

Please note that technical editing may introduce minor changes to the text and/or graphics, which may alter content. The journal's standard [Terms & Conditions](#) and the [Ethical guidelines](#) still apply. In no event shall the Royal Society of Chemistry be held responsible for any errors or omissions in this *Accepted Manuscript* or any consequences arising from the use of any information it contains.

COMMUNICATION

Highly fluorescent and bioresorbable polymeric nanoparticles with enhanced photostability for cell imaging

Cite this: DOI: 10.1039/x0xx00000x

Received 00th January 2012,

Accepted 00th January 2012

DOI: 10.1039/x0xx00000x

www.rsc.org/

Shuo Huang,^{†a} Shiyong Liu,^{†a} Kai Wang,^a Cangjie Yang,^a Yimin Luo,^a Yingdan Zhang,^{bc} Bin Cao,^{bd} Yuejun Kang,^{a,*} Mingfeng Wang^{a,*}

We report a facile and general strategy of enhancing the photostability of organic fluorophores for bioimaging applications. As a proof of concept, bright and robust fluorescence was observed in solid states of a well-defined synthetic polymer polycaprolactone consisting of di(thiophene-2-yl)-diketopyrrolopyrrole covalently linked in the middle of the polymer chain as a biocompatible and bioresorbable matrix. The nanoparticles prepared through a nanoprecipitation process of these polymers could be internalized by both tumor cells and stem cells with little cytotoxicity. Moreover, these highly fluorescent nanoparticles exhibited significantly enhanced photostability compared to commercial quantum dots or physical blends of dye/polymer complex in cell imaging and long-term tracing.

Introduction

Fluorescence imaging, due to its high specificity, sensitivity and imaging contrast, has proven to be an indispensable tool in modern biotechnology for advancing our understanding of various biological systems.¹⁻³ Among a variety of probes for fluorescence imaging, small organic fluorophores have been most widely used owing to their high fluorescence quantum yield, relatively low toxicity, and structural versatility that enables facile tuning of the optical properties and conjugation with biomolecules.³⁻⁷ For example, Alexa Fluor[®] family of fluorescent molecules has been commercially available and used as cell and tissue labels in fluorescence microscopy and cell biology. Another example is 4',6-diamidino-2-phenylindole, denoted as DAPI, which has been a commonly used fluorescent probe for selectively labeling of DNA in cell nucleus.

Despite these advantages, most organic fluorophores suffer from their poor photostability, i.e. the fluorescence intensity decays quickly (tens of seconds) under continuous exposure to light. This phenomenon, also called photobleaching, limits the ability of employing fluorescence microscopy or spectroscopy for long-term tracking of biological activities. Previous studies indicate that the formation of non-fluorescent triplet states (denoted as T₁), following the photonic excitation process, and the presence of molecular oxygen play a major role in the photobleaching of organic fluorophores. In air-saturated solutions, reactions between molecular oxygen and T₁ lead to substantial generation of reactive oxygen species (ROS), including HO•, HO₂•, and H₂O₂, and rapid photobleaching.

Several strategies such as oxygen depletion and addition of protective agents as triplet-state quenchers, although being able to reduce photobleaching to some extent, have achieved limited success in fluorescence-based bioimaging.³ Recently, Blanchard and coworkers⁸ have reported a strategy of covalently linking protective moieties (e.g. cyclooctatetraene, 4-nitrobenzyl alcohol, 6-hydroxy-2,5,7,8-tetramethylchroman-2-carboxylic acid) to cyanine fluorophores to enhance the photostability. Single-molecule fluorescence imaging showed remarkable enhancement of photostability in these modified fluorophores compared to the native ones without protective agents. Nevertheless, the improvement of photostability varies with different members of the cyanine class, suggesting the need for a deeper understanding of how the protective agents provide photostabilization.⁸ Relatively high photostability has been observed in inorganic semiconductor quantum dots,⁹⁻¹³ organic dye-silica core/shell NPs,^{14, 15} some organic and polymeric fluorescent dots,^{16, 17} and some optimized fluorescence proteins through mutagenesis.¹⁸ For example, enhanced photostability has been recently reported in nanoparticles composed of organic fluorophores with aggregation induced emission (AIE) effect,^{16, 19-21} but such improvement has been only observed in limited groups of organic dyes and polymers. Despite these recent advances, a general strategy of obtaining highly luminescent, photostable and non-

phototoxic fluorophores for long-term bioimaging is still in great demand.³

Herein we report a facile strategy of enhancing the photostability by covalently linking an organic fluorophore, di(thiophene-2-yl)-diketopyrrolopyrrole (DPP), in the middle of a biocompatible and bioresorbable polymer chain, polycaprolactone (PCL) (Fig. 1a). This polymer, denoted as PCL-DPP-PCL, has a number-average molecular weight (M_n) of 38,300 Da and a polydispersity index (M_w/M_n) of 1.98. In contrast to small-molecule DPP derivatives which often show dramatic fluorescence quenching in solid states due to significant intermolecular π - π aggregation, we found that PCL-DPP-PCL tethered with long PCL chains shows remarkably bright fluorescence in solid states, suggesting that the aggregation of DPP moieties is suppressed by the covalently attached PCL chains. In addition, PCL as a biocompatible and bioresorbable polyester has attracted much attention for use as an implantable biomaterial in tissue engineering and drug delivery.²² Biodegradation of PCL is slow compared to other polymers, thus making it suitable for long-term delivery extending over a period of more than one year.

We expected that the integration of strong fluorescence of DPP with the biophysical properties of PCL could make PCL-DPP-PCL an ideal fluorescence probe for bioimaging. Considering the hydrophobic nature of both DPP and PCL in this polymer, we used Pluronic[®] 127 as a surfactant and followed a method of nanoprecipitation to disperse PCL-DPP-PCL as nanoparticles (NPs) in aqueous media (Fig. 1a). The resulting NPs were highly fluorescent and showed remarkably enhanced photostability compared to commercial organic fluorophores in imaging of both human liver cancer cell line (HuH-7) and porcine mesenchymal stem cells (MSCs). Moreover, these polymeric NPs showed brighter and more robust fluorescence properties compared to commercially available imaging probes such as quantum dots (Qtracker[®]) in long-term tracing of cells.

Results and discussion

Preparation and characterization of NPs. Fig. 1a shows the molecular structure of PCL-DPP-PCL and a schematic presentation of the NPs formed through a nanoprecipitation process.²³⁻²⁶ In this process, an aliquot of PCL-DPP-PCL dissolved in tetrahydrofuran (THF) (3 mg/mL) was added to a vigorously stirred solution of Pluronic[®] 127 in water. Self-assembly was driven by the hydrophobic interaction between PCL-DPP-PCL and the polypropylene oxide (PPO) block of Pluronic[®] 127 which collapsed to form the core of the NPs. The shell of the NPs consists of PEG chains originated from Pluronic[®] 127 that extrude to the aqueous media to provide the colloidal stability.

A representative scanning electron microscopy (SEM) image (Fig. 1b) shows that the resulting particles appear spherical and uniform in size and shape. A statistical analysis of the particle size gives an average diameter of 51 ± 4 nm. Assuming a density of $1.14 \text{ g}\cdot\text{cm}^{-3}$ for PCL at room temperature and neglecting the contribution of Pluronic[®] 127 to the diameter of each NP, the estimated average mass of each NP ($d = 51$ nm) was 4.77×10^4 KDa, and that in average 1,240 polymer chains of PCL-DPP-PCL ($M_n = 38,300$ Da) existed in the core of each NP. While we observed that the size of the NPs could be tuned by changing the concentration of the polymer in THF, the following results and discussion will only focus on NPs with an average diameter of 51 nm, which has been recently demonstrated to be within the optimal size range in monodisperse drug-silica nanoconjugates for deep tissue penetration and high retention in tumors.²⁷ Fig. 1c shows that the internal structure of the

PCL-DPP-PCL NPs appeared amorphous as measured with transmission electron microscopy (TEM). In addition, the size and shape of the NPs measured with TEM were consistent with those measured with SEM. Fig. 1d shows the result of dynamic laser light scattering (DLS) measurement, which gives an average diameter of 110 nm for the NPs dispersed in water. The size difference observed using electron microscopy and DLS, which has also been observed for other soft-matter particles, reflects the fact that the polymer NPs existed as a colloidal and swollen state in aqueous media, while they collapse and shrink to smaller sizes after being dried in air and imaged under the high-vacuum condition of electron microscopy.

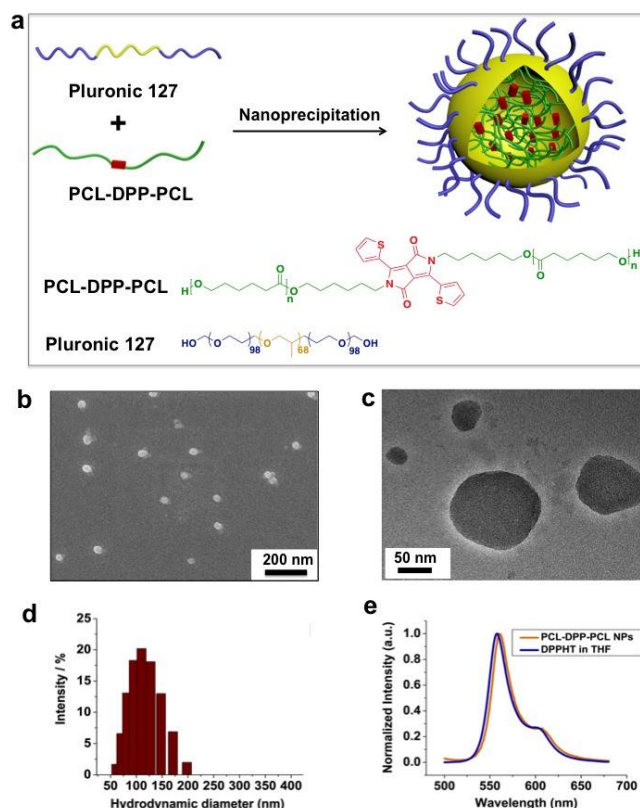


Fig. 1 (a) Schematic illustration of the preparation of PCL-DPP-PCL nanoparticles via nanoprecipitation process in the presence of Pluronic 127 as the stabilizer. (b-e) The morphology characterizations and optical properties of PCL-DPP-PCL nanoparticles: (b) The SEM image showing the average particle size of 51 ± 4 nm. (c) TEM image of PCL-DPP-PCL nanoparticles from a water suspension. (d) The dynamic light scattering test shows that the hydrated NPs have an average diameter of 110 nm in water suspension. (e) The fluorescence emission spectra of PCL-DPP-PCL nanoparticles (orange) and DPPHT in THF (blue) under 488 nm excitation.

Both the UV-vis absorbance (Fig. S1, Supporting Information) and emission spectra (Fig. 1e) of the PCL-DPP-PCL NPs appear similar to those of a small-molecule DPP derivative, [2,5-bis(6-hydroxyhexyl)-3,6-di(thiophen-2-yl)pyrrolo[3,4-c]pyrrole-1,4(2*H*,5*H*)-dione] (DPPHT) in dilute solution of THF. The NP dispersion in water shows characteristic absorbance peaks of DPP at 505 and 550 nm, respectively, despite some light-scattering effect (Fig. S1). The emission spectrum (Fig. 1e) of the PCL-DPP-PCL NP dispersion shows a major emission peak located at 560 nm, accompanied with a shoulder at 600 nm. There is a slight red shift (3 nm) of the maximum emission peak in the NP dispersion compared to that of DPPHT in THF. The fluorescence quantum yield of the PCL-DPP-PCL NPs in water is as high as 0.29, based on Rhodamine 6G (quantum yield = 0.95, in ethanol)²⁸ as the standard. These

results imply that the intermolecular π - π aggregation among DPP units is minimal in the core of the PCL-DPP-PCL NPs.

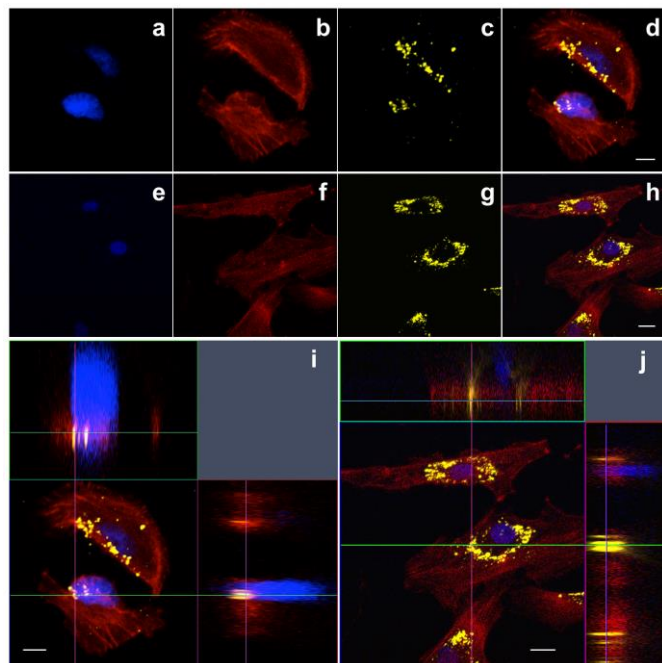


Fig. 2 Cellular uptake of PCL-DPP-PCL nanoparticles (NPs) in HuH-7 tumor cells (a-d and i) and MSCs (e-h and j) imaged by confocal laser scanning microscopy. The fluorescence of DAPI, Alexa Fluor[®] 633 phalloidin, and NPs are pseudo-labeled with blue (a, e), red (b, f), and yellow (c, g), respectively. Merged images of HuH-7 cells and MSCs from three channels are shown in (d) and (h), respectively. (i) and (j) are ortho-view images of z-stack, showing nanoparticles inside the cells. Scale bars: 10 μ m (HuH-7) and 20 μ m (MSC). For a, b, c, d, and i, pixel dwell time: 0.39 μ s; frame size: 1024 \times 1024; pixel size: 0.086 μ m. For e, f, g, h, and j, pixel dwell time: 1.00 μ s; frame size: 512 \times 512; pixel size: 0.45 μ m.

In vitro cellular uptake of NPs. To explore the potential of these NPs in bioimaging application, we first studied the cellular uptake *in vitro*. Two types of cell lines were chosen to this end. HuH-7 is a hepatocyte derived carcinoma cell line that has been used as a popular model for cancer research and some transfection study on hepatological infectious diseases.²⁹⁻³¹ MSCs are multipotent stromal cells that are able to differentiate into a variety of important cell lineages, and have become a promising cell source for regenerative medicine and tissue engineering.³² Therefore we believe these two types of cells are both representative and biomedically relevant to characterize the prepared PCL-DPP-PCL NPs for cell imaging. Fig. 2 shows the fluorescence images of these two types of cells observed from three channels corresponding to different fluorophores: blue (DAPI), yellow (PCL-DPP-PCL NPs), and red (Alexa Fluor[®] 633 phalloidin). The merged images from all three channels and the ortho-view of z-stack confirm that the NPs could be internalized by both HuH-7 tumor cells (Fig. 2 a-d, and i) and MSCs (Fig. 2 e-h, and j). Interestingly, the images in Fig. 2 (a-d, and i) suggest that the HuH-7 tumor cell nearly finished the mitotic (M) phase or cytokinesis when the mother cell split into two containing roughly equal shares of cellular components. As shown in Fig. 2, the internalized NPs are mainly located in the perinuclear cytoplasm, while not exhibiting obvious affinity to any specific intracellular organelle. For further applications targeting at specific subcellular compartments, it may be possible that the polymeric shell of these NPs could be functionalized with various ligands, such as nuclear localization signals (NLS) to facilitate NP passage through nuclear

pore complex (NPC) for gene delivery³³, or mitochondria-targeting probes to enhance specific drug delivery to mitochondria and improve the therapeutic efficacy.³⁴

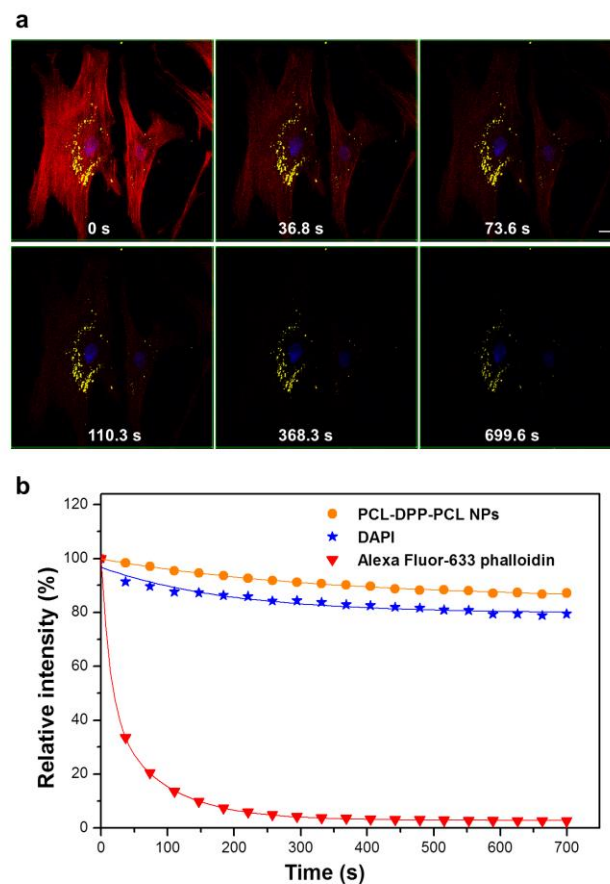


Fig. 3 Photostability of fluorescent PCL-DPP-PCL nanoparticles (NPs) compared to Alexa Fluor[®] 633 phalloidin and DAPI in MSC. The fluorescence of DAPI, NPs, and Alexa Fluor[®] 633 phalloidin are pseudo-labeled with blue, yellow and red, respectively. (a) Chronological decay of fluorescence intensity of a multiply-stained MSC at different time points imaged by confocal laser scanning microscopy. The whole image field was photobleached. Pixel dwell time: 0.50 μ s; frame size: 1024 \times 1024; pixel size: 0.28 μ m. Scale bar: 20 μ m. (b) Relative intensity (instantaneous intensity / initial intensity) change of three fluorophores in the photobleached region. Curves are fitted using mono-exponential (PCL-DPP-PCL NPs and DAPI) or bi-exponential functions (Alexa Fluor[®] 633 phalloidin). The nominal powers of 405, 561, and 633 nm lasers are 20 mW, 20 mW, and 5 mW, respectively.

Photostability of NPs in cellular imaging. Photobleaching is always a major concern in bioimaging applications of organic fluorophores. To characterize the photostability of PCL-DPP-PCL NPs, we compared their performance with two popular commercial fluorophores, DAPI and Alexa Fluor[®] 633 phalloidin, by a simultaneous photobleaching test for multiply-stained biological cells. After being stained with a cocktail of three dyes, MSCs were continuously exposed to 405, 561, and 633 nm laser irradiation and the fluorescence emission of each fluorophore was recorded at time points in 36.8-second intervals for a total duration of about 12 min. A band-pass filter combination was applied with bandwidths tuned to record the emission in three channels: blue (421-481 nm), yellow (569-621 nm), and red (650-758 nm). Fig. 3a and the time-lapse video (Supplementary Movie 1) show the merged images of the same multiply-stained MSC and the chronological decay of

fluorescence intensity. A more detailed time-lapse of photobleaching, including those recorded through three individual fluorescence channels, is provided in Fig. S2 and Supplementary Movie 2. It can be observed that all three fluorophores showed relatively high fluorescence intensity at the beginning of the test, while the subsequent photobleaching of three fluorophores were not synchronous. The fluorescence intensity of Alexa Fluor® 633 phalloidin decayed most rapidly and the F-actin cytoskeleton was barely detectable after 110 s (Fig. S2b). The fluorescence intensity of DAPI and NPs decreased much more slowly (Fig. S2c, d). Notably, the NPs were able to maintain strong fluorescence intensity during the test and maintain almost 90% of initial intensity even after 11 min (Fig. S2d).

A quantitative analysis of the relative intensity change (Fig. 3b) by curve fitting using exponential functions provided more insight of the decay kinetics of three different fluorophores. The PCL-DPP-PCL NPs exhibited mono-exponential decay expressed by $[y=A_1*\exp(-t/\tau_1)+y_0]$, where (A_1+y_0) represents the initial relative intensity, y_0 is the relative residual fluorescence intensity, and τ_1 is the decay rate constant called *mean lifetime*. The *half-life* was calculated as $\ln(2)*\tau_1$ (Table S1). DAPI also showed mono-exponential decay (Table S2) as reported in some previous studies.³⁵ Although there was no prior study reporting the decay kinetics of Alexa Fluor® 633 phalloidin, the fitting results showed that it could be described by a bi-exponential model $[y=A_1*\exp(-t/\tau_1)+A_2*\exp(-t/\tau_2)+y_0]$ (Table S3) in MSC. In this bi-exponential model, $(A_1+A_2+y_0)$ represent the initial relative intensity; the half-life was computed based on the longer *mean lifetime* (Table S3). A comparison of the half-life values of three fluorophores in MSC (Tables S1-S3) clearly showed that NPs (230 s) exhibited significantly higher photostability compared to DAPI (132 s) and Alexa Fluor® 633 phalloidin (58.6 s).

As discussed previously, small-molecule DPP derivatives often show fluorescence quenching in solid states due to significant intermolecular π - π aggregation. The reason why PCL-DPP-PCL NPs exhibit much greater photostability could be due to the covalent bonds between DPP and PCL chains, which efficiently suppressed the aggregation of DPP molecules. In order to verify this hypothesis, we prepared PCL/DPPHT nanoparticles (Fig. S3 a-c) by simple physical blending (i.e. without any covalent bond formation between these two components) of DPPHT (8.0×10^{-4} mmol) and PCL ($M_n = 22,000$, PDI = 1.3) with a weight ratio similar to that of PCL-DPP-PCL. These physically blended PCL/DPP NPs could also be internalized by MSCs and accumulated in perinuclear region (Fig. S4 a-d, and i). However, photobleach test revealed that these physically blended NPs exhibited much weaker photostability (Fig. S5) as compared to the covalently bonded PCL-DPP-PCL NPs (Fig. 3). After 125 s of laser irradiation (561 nm), physically blended NPs could only retain about 13% of initial fluorescence intensity.

In addition to DPP-based fluorophores, this strategy to enhance the photostability could also be applied to other fluorophores with different excitation and emission wavelengths. As an example, we chose a quinacridone (QA) derivative (Fig. S3g) as an initiator and synthesized PCL-QA-PCL NPs using a method similar to the preparation of PCL-DPP-PCL NPs. The SEM image (Fig. S3d) showed that the resulting spherical particles had an average diameter of 117 ± 21 nm, which was consistent with the DLS (Fig. S3f) and TEM (Fig. S3e) results. Fluorescence microscopy (Fig. S4 e-h, and j) showed that they could be uptaken by MSCs and accumulated in the perinuclear region. The photobleach test suggested that the photostability of PCL-QA-PCL NPs (Fig. S6) was relatively weaker

than that of PCL-DPP-PCL NPs (Fig. 3), which could be due to different properties of QA and DPP.

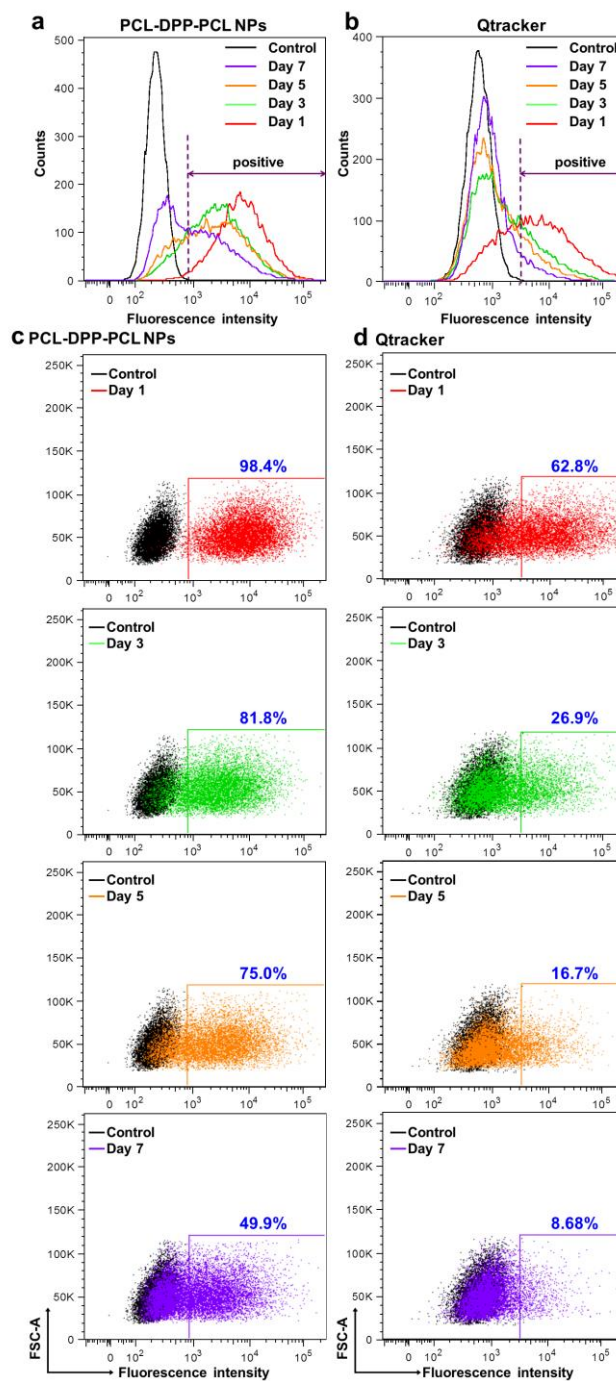


Fig. 4 Long-term tracing of HuH-7 tumor cells using (a, c) PCL-DPP-PCL nanoparticles and (b, d) Qtracker®. The fluorescence intensity change of the labeled cells was measured by flow cytometry analyses at different time points. The control represents the unlabeled cells. The percentages of cells retaining strong fluorescence in (c, d) were determined according to the gating thresholds as indicated in (a, b) for NP and Qtracker®, respectively.

Long-term cell tracing using PCL-DPP-PCL NPs vs. Qtracker®. In addition to the photostability of fluorophore upon exposure to light, prior studies have suggested that the decrease of fluorescence intensity of stained cells in long-term study could be also due to loss of fluorophores during cell division and exocytosis³⁷. Therefore we

investigated the application of PCL-DPP-PCL NPs for long-term cell tracing by fluorescence imaging, and compared their performance with a commercial counterpart, the Qtracker[®] cell labeling kit consisting of highly fluorescent quantum dot nanocrystals (nanoscale atom clusters comprising a core, a shell and surface coating).

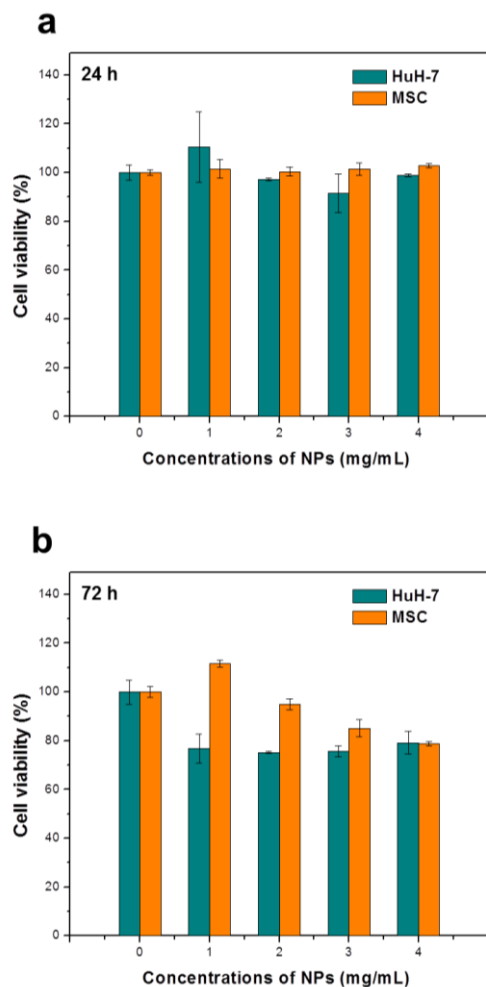


Fig. 5 Cell viabilities of HuH-7 and MSCs after incubating with different concentrations of PCL-DPP-PCL NPs for (a) 24 h and (b) 72 h tested by PrestoBlue assay. Cells without treatment by NPs were used as control. Values were expressed as means \pm SD ($n=3$). Paired student t-test was used for statistical analysis between groups treated with different concentrations of NPs and control ($p>0.5$).

HuH-7 tumor cells were firstly incubated with NPs and Qtracker[®] for 48 h at concentration of 2 nM, respectively. Then the excess fluorophores were removed and washed by $1\times$ PBS. The cells were then subcultured into a 6-well plate and cultured for up to 7 days. The fluorescence change of the labeled cells was monitored by fluorescence microscopy (Fig. S7) and quantitatively analyzed at specific time points by flow cytometry for about 10,000 cell events in each test (Fig. 4). The fluorescence of HuH-7 cells labeled with either NPs or Qtracker[®] gradually decayed and shifted from the high intensity spectrum (Day 1) toward the weak intensity regime (Day 7). It was noted that the NP-labeled tumor cells exhibited much higher fluorescence stability with 49.9% of the population remaining to be strongly fluorescent at Day 7; whereas only 8.68% of the Qtracker[®]-labeled cells maintained their fluorescence at Day 7. Similar comparative study was also performed with MSC culture for

up to 14 days (Fig. S8). The flow cytometry analysis and fluorescence microscopy again demonstrated the impressive long-term photostability of this PCL-DPP-PCL NP system, with 46.7% of the NP-stained MSCs retaining strong fluorescence after 2 weeks. These results indicate that the PCL-DPP-PCL NPs are highly advantageous as a stable fluorophore particularly for applications related to long-term cell tracing.

Cytotoxicity of PCL-DPP-PCL NPs. Finally, we evaluated the cytotoxicity of the PCL-DPP-PCL NPs using PrestoBlue assay. Resazurin ($\lambda_{\text{max,abs}} = 600$ nm) in PrestoBlue[®] reagent, a nonfluorescent blue compound, can be reduced in live cells by metabolism to resorufin ($\lambda_{\text{max,abs}} = 571$ nm), which is red in color and highly fluorescent. Since the number of metabolically active cells proportionally correlates with the reduction level, the absorbance readings can be converted and expressed as the percentage reduction of the PrestoBlue reagent, indicating the relative cell viability. HuH-7 tumor cells and MSCs were incubated with NPs of different concentrations (up to 4 mg/mL) for 24 h and 72 h. Percentage reduction of PrestoBlue reagent in each sample was measured with regard to that in cell culture without NP staining (the control). Fig. 5 shows that the cell viability of MSCs and HuH-7 cells was not significantly affected for up to 72 h, indicating minimum cytotoxicity of the PCL-DPP-PCL NPs. Statistical analysis by paired student t-test indicated that there was no significant difference between groups treated with different concentrations of NPs and the control for both HuH-7 and MSCs ($p>0.5$).

Conclusions

In summary, we have presented a new type of highly fluorescent and bioresorbable polymeric NPs prepared through nanoprecipitation of a well-defined polymer, PCL-DPP-PCL, in the presence of Pluronic[®] 127 as the stabilizer. A key feature of our molecular design lies in the covalent insertion of DPP as a highly fluorescent moiety into the middle of each PCL chain. Such covalent bonding at the interface of DPP and PCL as well as the steric effect endowed by long PCL chains effectively suppress the π - π aggregation of DPP in the PCL matrix. As a consequence, PCL-DPP-PCL with M_n of 38,300 Da showed bright fluorescence in solid states. The NPs prepared through a nanoprecipitation process were highly fluorescent and could be internalized by both HuH-7 tumor cells and MSCs with little cytotoxicity to these cells. Most importantly, the PCL-DPP-PCL NPs exhibited significantly enhanced photostability compared to several commercial organic fluorophores, the physically blended DPPHT/PCL NPs and Qtracker[®] for imaging of both tumor cells and stem cells. These unique properties make the PCL-DPP-PCL NPs promising imaging probes to track a broad range of biological systems. Compared to previously reported fluorescent organic or polymeric NPs,^{16, 17} the 1.3% weight fraction of fluorescent components in these NPs is significantly lower and the polymer matrix (i.e. PCL) has proved to be biocompatible and bioresorbable. Therefore the potential toxicity, if any, caused by the encapsulated fluorophores is minimized. Moreover, the fluorescence excitation and emission wavelengths of these synthetic NPs can be customized and finely tuned during synthesis for specific applications. Currently we are extending this strategy to polymers with strong fluorescence in near infrared range that is important for *in-vivo* imaging.

Acknowledgement

M.W. is grateful to the funding support by a start-up grant from Nanyang Technological University, AcRF Tier 1 (RG49/12) and AcRF Tier 2 (ARC 36/13) from the Ministry of Education, Singapore. Y.K. acknowledges the AcRF Tier 2 (ARC 22/13) from the Ministry of Education, Singapore. B.C. acknowledges the funding support from Singapore Centre on Environmental Life Sciences Engineering (SCELSE, M4330005.C70). S.H., S.L. and K.W. gratefully acknowledge the Ph.D. research scholarships from Nanyang Technological University.

Notes and references

^aSchool of Chemical and Biomedical Engineering, Nanyang Technological University, 62 Nanyang Drive, Singapore 637459. E-mail: Y. Kang (yuejun.kang@ntu.edu.sg); M. Wang (mfwang@ntu.edu.sg)

^bSingapore Centre for Environmental Life Sciences Engineering, Nanyang Technological University, Singapore.

^cInterdisciplinary Graduate School, Nanyang Technological University, Singapore.

^dSchool of Civil and Environmental Engineering, Nanyang Technological University, Singapore.

†These authors contributed equally to this work.

Electronic Supplementary Information (ESI) available: [Experimental procedures, absorbance spectra, confocal microscopy characterization]. See DOI: 10.1039/c000000x/

1. in *Principles of Fluorescence Spectroscopy*, ed. J. Lakowicz, Springer US, Editon edn., 2006.
2. P.-C. Cheng, in *Handbook of Biological Confocal Microscopy*, ed. J. B. Pawley, Springer US, New York, Editon edn., 2006, pp. 162-206.
3. Q. Zheng, M. F. Juette, S. Jockusch, M. R. Wasserman, Z. Zhou, R. B. Altman and S. C. Blanchard, *Chem. Soc. Rev.*, 2014, **43**, 1044-1056.
4. A. Kaeser and A. P. H. J. Schenning, *Adv. Mater.*, 2010, **22**, 2985-2997.
5. G. T. Dempsey, J. C. Vaughan, K. H. Chen, M. Bates and X. Zhuang, *Nat. Methods*, 2011, **8**, 1027-1036.
6. A. Wagh, S. Y. Qian and B. Law, *Bioconjug. Chem.*, 2012, **23**, 981-992.
7. A. Reisch, P. Didier, L. Richert, S. Oncul, Y. Arntz, Y. Mély and A. S. Klymchenko, *Nat. Commun.*, 2014, **5**, 4089.
8. R. B. Altman, D. S. Terry, Z. Zhou, Q. Zheng, P. Geggier, R. A. Kolster, Y. Zhao, J. A. Javitch, J. D. Warren and S. C. Blanchard, *Nat. Methods*, 2012, **9**, 68-71.
9. M. Bruchez, M. Moronne, P. Gin, S. Weiss and A. P. Alivisatos, *Science*, 1998, **281**, 2013-2016.
10. W. C. W. Chan and S. Nie, *Science*, 1998, **281**, 2016-2018.
11. X. Wu, H. Liu, J. Liu, K. N. Haley, J. A. Treadway, J. P. Larson, N. Ge, F. Peale and M. P. Bruchez, *Nat. Biotechnol.*, 2003, **21**, 41-46.
12. Q. Liu, B. Guo, Z. Rao, B. Zhang and J. R. Gong, *Nano Lett.*, 2013, **13**, 2436-2441.
13. L. A. Osminkina, K. P. Tamarov, A. P. Sviridov, R. A. Galkin, M. B. Gongalsky, V. V. Solovyev, A. A. Kudryavtsev and V. Y. Timoshenko, *J. Biophotonics*, 2012, **5**, 529-535.
14. A. Burns, H. Ow and U. Wiesner, *Chem. Soc. Rev.*, 2006, **35**, 1028-1042.
15. H. Ow, D. R. Larson, M. Srivastava, B. A. Baird, W. W. Webb and U. Wiesner, *Nano Lett.*, 2005, **5**, 113-117.
16. W. Qin, K. Li, G. Feng, M. Li, Z. Yang, B. Liu and B. Z. Tang, *Adv. Funct. Mater.*, 2013, **24**, 635-643.
17. C. Wu and D. T. Chiu, *Angew. Chem. Int. Ed.*, 2013, **52**, 3086-3109.
18. N. C. Shaner, M. Z. Lin, M. R. McKeown, P. A. Steinbach, K. L. Hazelwood, M. W. Davidson and R. Y. Tsien, *Nat. Methods*, 2008, **5**, 545-551.
19. K. Li, W. Qin, D. Ding, N. Tomczak, J. Geng, R. Liu, J. Liu, X. Zhang, H. Liu, B. Liu and B. Z. Tang, *Sci. Rep.*, 2013, **3**, 1150.
20. Q. Zhao, K. Li, S. Chen, A. Qin, D. Ding, S. Zhang, Y. Liu, B. Liu, J. Z. Sun and B. Z. Tang, *J. Mater. Chem.*, 2012, **22**, 15128-15135.
21. C. W. T. Leung, Y. Hong, S. Chen, E. Zhao, J. W. Y. Lam and B. Z. Tang, *J. Am. Chem. Soc.*, 2012, **135**, 62-65.
22. M. A. Woodruff and D. W. Hutmacher, *Prog. Polym. Sci.*, 2010, **35**, 1217-1256.
23. J.-S. Hu, Y. Guo, H.-P. Liang, L.-J. Wan and L. Jiang, *J. Am. Chem. Soc.*, 2005, **127**, 17090-17095.
24. M. Akbulut, P. Ginart, M. E. Gindy, C. Theriault, K. H. Chin, W. Soboyejo and R. K. Prud'homme, *Adv. Funct. Mater.*, 2009, **19**, 718-725.
25. X. Zhang, C. Dong, J. A. Zapien, S. Ismathullakhan, Z. Kang, J. Jie, X. Zhang, J. C. Chang, C.-S. Lee and S.-T. Lee, *Angew. Chem. Int. Ed.*, 2009, **48**, 9121-9123.
26. F. Bai, Z. Sun, H. Wu, R. E. Haddad, E. N. Coker, J. Y. Huang, M. A. Rodriguez and H. Fan, *Nano Lett.*, 2011, **11**, 5196-5200.
27. L. Tang, X. Yang, Q. Yin, K. Cai, H. Wang, I. Chaudhury, C. Yao, Q. Zhou, M. Kwon, J. A. Hartman, I. T. Dobrucki, L. W. Dobrucki, L. B. Borst, S. Lezmi, W. G. Heflerich, A. L. Ferguson, T. M. Fan and J. Cheng, *PNAS*, 2014, **111**, 15344-15349.
28. R. F. Kubin and A. N. Fletcher, *J. Lumin.*, 1982, **27**, 455-462.
29. L. Z. Chen, J. M. Zheng, Y. Zhang, L. X. Yang, J. Q. Wang, J. Ni, D. X. Cui, C. Q. Yu and Z. L. Cai, *Mol. Ther.*, 2011, **19**, 1521-1528.
30. G. K. Wilson and Z. Stamataki, *Int. J. Hepatol.*, 2012, **2012**, 292591.
31. T. Kato, M. Tanaka and M. Oba, *Plos One*, 2013, **8**.
32. P. Bianco, X. Cao, P. S. Frenette, J. J. Mao, P. G. Robey, P. J. Simmons and C. Y. Wang, *Nat. Med.*, 2013, **19**, 35-42.
33. K. Ma, H. Shen, S. Shen, M. Xie, C. Mao, L. Qiu and Y. Jin, *J. Gene Med.*, 2011, **13**, 290-301.
34. S. V. Boddapati, G. G. M. D'Souza, S. Erdogan, V. P. Torchilin and V. Weissig, *Nano Lett.*, 2008, **8**, 2559-2563.
35. M. L. Barcellona and E. Gratton, *Eur. Biophys. J.*, 1990, **17**, 315-323.
36. G. Cosa, K. S. Focsaneanu, J. R. N. McLean, J. P. McNamee and J. C. Scaiano, *Photochem. Photobiol.*, 2001, **73**, 585-599.
37. Y. Gao, Y. Cui, J. K. Chan and C. Xu, *Am. J. Nucl. Med. Mol. Imaging*, 2013, **3**, 232-246.

Journal Name

RSCPublishing

COMMUNICATION

Nanoscale Accepted Manuscript